Original Article

Latin American Journal of Solids and Structures
www.lajss.org

Effect of Loose Bonding and Corrugated Boundary Surface on Propagation of Rayleigh-Type Wave

Abstract

The problems concerns to the propagation of surface wave propagation through various anisotropic mediums with initial stress and irregular boundaries are of great interest to seismologists, due to their applications towards the stability of the medium. The present paper deals with the propagation of Rayleigh-type wave in a corrugated fibre-reinforced layer lying over an initially stressed orthotropic half-space under gravity. The upper free surface is assumed to be corrugated; while the interface of the layer and half-space is corrugated as well as loosely bonded. The frequency equation is deduced in closed form. Numerical computation has been carried out which aids to plot the dimensionless phase velocity against dimensionless wave number for sake of graphical demonstration. Numerical results analyze the influence of corrugation, loose bonding, initial stress and gravity on the phase velocity of Rayleigh-type wave. Moreover, the presence and absence of corrugation, loose bonding and initial stress is also discussed in comparative manner.

Keywords

Rayleigh-type wave, initial stress, gravity, loosely bonded, corrugation, fibre-reinforced, orthotropic

Abhishek Kumar Singh [a]
Kshitish Ch. Mistri [a,*]
Mukesh Kumar Pal [a]

[a] Department of Applied Mathematics, IIT(ISM), Dhanbad-826004
Email: abhi.5700@gmail.com, kchmistri@gmail.com, 3007mukesh@gmail.com

* Corresponding author

http://dx.doi.org/10.1590/1679-78253577

Received 02.12.2016
In revised form 28.09.2017
Accepted 29.09.2017
Available online 30.09.2017

NOMENCLATURE

H = The average width of the layer
$f_i(x)$ = Periodic functions and independent of y .
$R_l^{(j)}, I_l^{(j)}$ = The cosine and sine Fourier coefficients respectively.
b = The wavenumber associated with corrugated boundary surfaces.
a_1, a_2 = The amplitudes of corrugation.
u_1, u_2, u_3 = The displacement components of fibre-reinforced layer along x, y, z direction respectively.
u_1^*, u_2^*, u_3^* = The displacement components of orthotropic half-space along x, y, z direction respectively.
$\vec{a} = \left(a_1^*, a_2^*, a_3^*\right)$ the preferred direction of reinforcement.
τ_{ij} = The components of stress of layer.
e_{ij} = The components of infinitesimal strain of layer.
δ_{ij} = Kronecker delta.
μ_T = Transverse shear modulus of layer.
μ_L = Longitudinal shear modulus of layer.
α, β = Specific stress components for concrete part of the composite material.
λ = Lame's constant of elasticity.
P =Initial compression in x -direction.
ρ_1, ρ_2 = Medium density,
τ_{ij}^* =The stress components of half-space.

ω_{ij}^{*} = The rotational components of half-space.

C_{ij} = Stiffness tensor components in contraction notation.

G = Biot's gravity parameter.

Ω = Bonding parameter.

1 INTRODUCTION

The problems of elastodynamics are not limited to the mechanics of those elastic materials which are simply isotropic, rather the problems take a more general and realistic form when the media considered are anisotropic. The presence of some effective physical factors namely initial stress, hydrostatic stress, cracks, fractures, etc. causes the mediums to behave anisotropically to the propagation of waves through it. These initial stresses (tensile/compressive) are the results of overburdened layer, atmospheric pressure, variation in temperature, slow process of creep and gravitational field. Tensile stress is said to responsible for more rigidity and compressive stress for less rigidity of a medium. On the other hand, presence of fibre-reinforced materials in earth's crust, in the form of hard or soft rocks may also affect the wave propagation. These composite materials adopt self-reinforced behavior under certain temperature and pressure. It finds numerous applications in construction, civil engineering, geophysics and geomechanics due to its low weight and high strength. The reinforcement of soil, both naturally and synthetically, enhances the strength and load bearing capacity of it. The mechanical behavior of composite materials could be well understood through the study of anisotropic elasticity. Carbon, nylon or conceivable metal whiskers, etc. are good models of fibre-reinforced materials. Prikazchikov and Rogerson [2003] studied the effect of pre-stress on the propagation of small amplitude waves in an incompressible, transversely isotropic elastic solid. Prosser and Green [1990] calculated some of the nonlinear (third order) moduli of T300/5208 graphite/ epoxy composite by measuring the normalized change in ultrasonic "natural" velocity as a function of stress and temperature. A lot of information about such reinforced materials can be gained from Spencer [1972] who analyses the macroscopic properties of fiber-reinforced materials. In the recent past, Chattopadhyay and Singh [2012] studied the propagation of horizontally polarised shear waves in an internal irregular (rectangular and parabolic irregularity) magnetoelastic self-reinforced stratum sandwiched between two semi-infinite magnetoelastic self-reinforced media. Some more important works include Fan and Hwu [1998], Grünewald et al. [2012], Chattopadhyay and Singh [2013], Chattopadhyay et al. [2010], Samal and Chattaraj [2011], Sethi et al. [2016], Abd-Alla [1999] and Gaur and Rana [2014].

Another important class of material which may be considered in the study of elastodynamic problems is the orthotropic material. The mechanical properties of such materials are unique and independent in three mutually perpendicular directions. Sometimes some fiber-reinforced composites imitate orthotropic materials.

Chai and Wu [1996] extended the Barnett-Lothe's integral formalism in order to determine the velocities of surface waves propagating in a pre-stressed anisotropic crystal. Singh and Yadav [2013] dealt with the reflection of qP and qSV waves at a free surface of a perfectly conducting transversely isotropic elastic solid half-space under initial stress. Using Rayleigh's method of approximation, the reflection and transmission of plane qP-wave at a corrugated interface between two dissimilar pre-stressed elastic solid half-spaces was discussed by Singh and Tomar [2008]. A tremendous amount of knowledge can be gathered regarding the effect of gravity on the propagation of waves from Biot [1965]; and also through some papers including Das et al. [1992] and Chattopadhyay et al. [2009]. Moreover, Kumar and Kumar [2011], Destrade [2001] and Chow [1971] have also contributed considering an orthotropic material medium in their study.

Changing medium may affect the wave propagation; intimating that the boundary surfaces (free boundary or interface) of mediums play important role in the study of wave propagation through different mediums. It is not necessary that the boundary surface always acquire a regular planar shape. While dealing with different elastodynamical problems, one may encounter boundary surfaces of different shapes. For example, the boundaries may possess a rectangular or parabolic irregularity; or it may be corrugated. Corrugated boundary surface may be defined as a series of parallel ridges and furrows. The undulatory factor of such boundaries affects the propagation of waves and vibrations. Further, the interface of two mediums may not be always welded rather it may be loosely bounded too.

The study of corrugated boundary surfaces and loosely bonded interfaces of material mediums is also important to understand the behavior of wave propagation. Starting with Tomar and Kaur [2007], Singh [2011, 2014], Singh and Kumar [1998], Khurana and Vashisth [2001], continued to Nandal and Saini [2013] and Singh et al. [2015] had studied the propagation of waves through corrugated boundary surfaces and loosely bonded interfaces.

The current study investigates the propagation of Rayleigh-type wave in a fibre-reinforced layer overlying an initially stressed orthotropic half-space under gravity. The upper free surface is assumed to be corrugated; while the interface of the layer and half-space is corrugated as well as loosely bonded. The closed form expression of frequency equation is derived and numerical computation for phase velocity is performed which is reflected graphically. The effect of corrugation, loose bonding, initial stress and gravity on the phase velocity of Rayleigh-type wave is highlighted in the study.

2 FORMULATION AND SOLUTION OF THE PROBLEM

Consider the propagation of Rayleigh-type wave in a fibre-reinforced layer lying over an initially stressed orthotropic half-space under gravity where the upper free surface is corrugated and the interface of the layer and half-space is corrugated as well as loosely bonded. The average width of the layer is assumed to be H. Cartesian co-ordinate system is chosen in such a way that x-axis is the direction of wave propagation, z-axis is positively pointing downwards and the origin is at the interface of the layer and half-space. The said geometry is illustrated in Fig. 1.

Let the equation of uppermost corrugated boundary surface be $z = f_2(x) - H$ and the equation of corrugated interface between layer and half-space be $z = f_1(x)$, where $f_1(x)$ and $f_2(x)$ are periodic functions and independent of y. Taking a suitable origin of coordinates we can represent Trigonometric Fourier series of. $f_1(x)$., $f_2(x)$ as follows (Asano, [1966]):

$$f_j = \sum_{l=1}^{\infty}\left[f_l^{(j)} e^{ilbx} + f_{-l}^{(j)} e^{-ilbx} \right], \quad j = 1, 2, \tag{1}$$

where $f_l^{(j)}$ and $f_{-l}^{(j)}$ are Fourier expansion coefficients and l is series expansion order. Let us introduce the constants $a_1, a_2, R_l^{(j)}, I_l^{(j)}$ as follows:

$$f_{\pm 1}^{(1)} = \frac{a_1}{2},\ f_{\pm 1}^{(2)} = \frac{a_2}{2},\ f_{\pm l}^{(j)} = \frac{R_l^{(j)} \mp i I_l^{(j)}}{2},\ j = 1, 2, \text{ and } l = 2, 3, \ldots$$

and

$$f_1 = a_1 \cos bx + R_2^{(1)} \cos 2bx + I_2^{(1)} \sin 2bx + \ldots + R_l^{(1)} \cos lbx + I_l^{(1)} \sin lbx + \ldots,$$
$$f_2 = a_2 \cos bx + R_2^{(2)} \cos 2bx + I_2^{(2)} \sin 2bx + \ldots + R_l^{(2)} \cos lbx + I_l^{(2)} \sin lbx + \ldots,$$

where $R_l^{(j)}, I_l^{(j)}$ are the cosine and sine Fourier coefficients respectively. As far the present problem is concerned, the corrugated upper boundary surface and lower boundary surface may be expressed with the aid of cosine terms i.e. $f_1 = a_1 \cos bx$ and $f_2 = a_2 \cos bx$ respectively, where b is the wavenumber associated with corrugated boundary surfaces, a_1 and a_2 are the amplitudes of corrugation and the wavelength of the corrugation is $2\pi / b$.

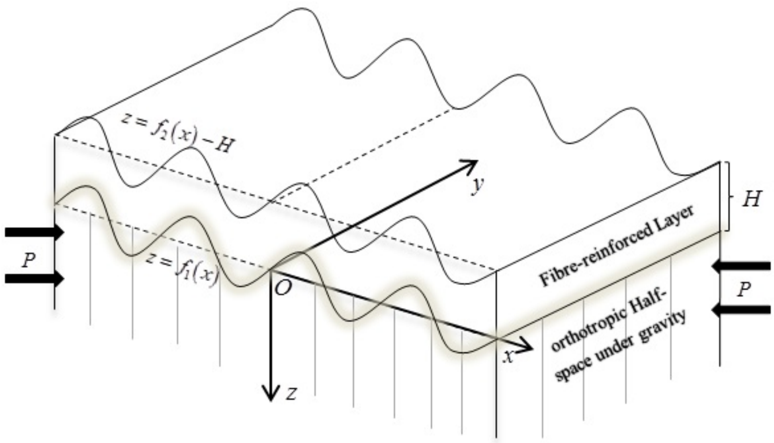

Figure 1: Typical structure of analysis.

Let us assume (u_1, u_2, u_3) and (u_1^*, u_2^*, u_3^*) as the displacement components of upper fibre-reinforced layer and lower initially stressed orthotropic half-space under gravity respectively.

3 GOVERNING EQUATIONS AND SOLUTION OF THE PROBLEM

For the propagation of Rayleigh-type wave, we consider

$$\begin{aligned} u_1 &= u_1(x,z,t),\ u_2 = 0,\ u_3 = u_3(x,z,t), \\ u_1^* &= u_1^*(x,z,t),\ u_2^* = 0,\ u_3^* = u_3^*(x,z,t), \end{aligned} \tag{2}$$

and the condition for plain strain deformation in xz -plane is $\partial_y = 0$.

Here we denote the partial derivative with respect to a variable $x_i\left(i=1,2,3\right)$ by ∂_i. The first and second time derivative are represented as ∂_t and ∂_{tt} respectively. Moreover, d_x and d_{xx} stands for $\frac{d}{dx}$ and $\frac{d^2}{dx^2}$ respectively.

3.1 Dynamics of Fibre-Reinforced Material

The constitutive equation for a fibre-reinforced linearly elastic anisotropic medium with preferred direction $\vec{a}$ is given by (Spencer [1972])

$$\tau_{ij} = \lambda e_{kk}\delta_{ij} + 2\mu_T e_{ij} + \alpha\left(a_k^* a_m^* e_{km}\delta_{ij} + a_i^* a_j^* e_{kk}\right) + 2\left(\mu_L - \mu_T\right)\left(a_i^* a_k^* e_{kj} + a_j^* a_k^* e_{ki}\right) + \beta a_k^* a_m^* e_{km} a_i^* a_j^*, \quad i,j,k,m = 1,2,3. \tag{3}$$

where τ_{ij} are the components of stress, $e_{ij} = \frac{1}{2}\left(\partial_j u_i + \partial_i u_j\right)$ are the components of infinitesimal strain, δ_{ij} is Kronecker delta, $\vec{a} = \left(a_1^*, a_2^*, a_3^*\right)$, which may be function of position, is the preferred direction of reinforcement such that $\sum_{i=1}^{3}\left(a_i^*\right)^2 = 1$. Indices take the values 1, 2, 3 and summation convention is employed. α, β and $\left(\mu_L - \mu_T\right)$ are reinforcement parameters. μ_T and μ_L can be identified as the transverse shear and longitudinal shear modulus in the preferred directions respectively. α, β are specific stress components to take into account different layers for concrete part of the composite material, λ is Lame's constant of elasticity.

Now, the equations of motion without body force are

$$\tau_{ij,j} = \rho_1 \partial_{tt} u_i \tag{4}$$

where ρ_1 stands for mass density.

Using Equations (2) and (3), Equation (4) reduces to

$$P_1\,\partial_{xx}u_1 + Q_1\,\partial_{xz}u_3 + R_1\partial_{zz}u_1 = \rho_1\partial_{tt}u_1, \tag{5}$$

$$R_1\partial_{xx}u_3 + Q_1\,\partial_{xz}u_1 + P_2\partial_{zz}u_3 = \rho_1\partial_{tt}u_3, \tag{6}$$

where

$$P_1 = \lambda + 2\alpha + \beta + 4\mu_L - 2\mu_T, Q_1 = \lambda + \alpha + \mu_L, P_2 = \lambda + 2\mu_T, R_1 = \mu_L.$$

Assume the solution of Equations (5) and (6) as

$$u_1 = A\ell_1 e^{-\gamma kz + ik(x-ct)}, \quad u_3 = A\ell_3 e^{-\gamma kz + ik(x-ct)}, \tag{7}$$

where $(\ell_1, 0, \ell_3)$ are the unit displacement vector components.

In view of Equation (7), Equations (5) and (6) yields

$$(\gamma^2\mu_L + \rho_1 c^2 - P_1)\ell_1 - i\gamma Q_1\ell_3 = 0, \tag{8}$$

$$-i\gamma Q_1\ell_1 + (\gamma^2 P_2 + \rho_1 c^2 - R_1)\ell_3 = 0. \tag{9}$$

For non-trivial solution of Equations (8) and (9), it follows that

$$\mu_L P_2\gamma^4 + m\gamma^2 + n = 0, \tag{10}$$

where

$$\gamma^2 = \frac{-m \pm \sqrt{m^2 - 4\mu_L P_2 n}}{2\mu_L P_2}, \quad m = \mu_L(\rho c^2 - \mu_L) + P_2(\rho_1 c^2 - P_1) + Q_1^2, \quad n = (\rho_1 c^2 - \mu_L)(\rho_1 c^2 - R_1), \tag{11}$$

so that, Equations (7) and (8) gives

$$\frac{u_3}{u_1} = \frac{\gamma_j^2 \mu_L + \rho_1 c^2 - P_1}{i\gamma_j Q_1} = \varsigma_j, \quad j = 1,2 .$$

Therefore, the displacement components of the upper Fibre-reinforced layer for propagation of Rayleigh-type wave are found as

$$u_1 = (A_1 e^{-k\gamma_1 z} + A_2 e^{-k\gamma_2 z} + A_3 e^{k\gamma_1 z} + A_4 e^{k\gamma_2 z}) e^{ik(x-ct)}, \tag{12}$$

$$u_3 = \left[\varsigma_1 (A_1 e^{-k\gamma_1 z} - A_3 e^{k\gamma_1 z}) + \varsigma_2 (A_2 e^{-k\gamma_2 z} - A_4 e^{k\gamma_2 z}) \right] e^{ik(x-ct)}. \tag{13}$$

3.2 Dynamics of the Lower Initially Stressed Orthotropic Half-Space under Gravity

The dynamical equations of motion for an elastic medium under gravity and initial compression stress P in x-direction are

$$\partial_x \tau_{11}^* + \partial_y \tau_{12}^* + \partial_z \tau_{13}^* + P\left(\partial_y \omega_{12}^* - \partial_z \omega_{13}^*\right) - \rho_2 g \partial_x u_3^* = \rho_2 \partial_{tt} u_1^*, \tag{14}$$

$$\partial_x \tau_{12}^* + \partial_y \tau_{22}^* + \partial_z \tau_{23}^* + P \partial_x \omega_{12}^* = \rho_2 \partial_{tt} u_2^*, \tag{15}$$

$$\partial_x \tau_{13}^* + \partial_y \tau_{23}^* + \partial_z \tau_{33}^* - P \partial_x \omega_{12}^* + \rho_2 g \partial_x u_1^* = \rho_2 \partial_{tt} u_3^*, \tag{16}$$

where ρ_2 is the medium density, τ_{ij}^* are the stress components and $\omega_{ij}^* = \frac{1}{2}\left(\partial_j u_i^* - \partial_i u_j^*\right)$ are the rotational components.

For the propagation of Rayleigh-type wave, Equations (14), (15) and (16) with the aid of Equation (2), leads to

$$\partial_x \tau_{11}^* + \partial_z \tau_{13}^* - P \partial_z \omega_{13}^* - \rho_2 g \partial_x u_3^* = \rho_2 \partial_{tt} u_1^*, \tag{17}$$

$$\partial_x \tau_{13}^* + \partial_z \tau_{33}^* - P \partial_x \omega_{13}^* + \rho_2 g \partial_x u_1^* = \rho_2 \partial_{tt} u_3^*. \tag{18}$$

The stress components τ_{ij}^* in this case can be written as:

$$\tau_{11}^* = \left(C_{11} + P\right) \partial_x u_1^* + \left(C_{13} + P\right) \partial_z u_3^*, \tag{19}$$

$$\tau_{22}^* = C_{13} \partial_x u_1^* + C_{33} \partial_z u_3^*, \tag{20}$$

$$\tau_{13}^* = \frac{1}{2}\left(C_{11} - C_{13}\right)\left(\partial_z u_1^* + \partial_x u_3^*\right), \tag{21}$$

where C_{ij} are stiffness tensor components in contraction notation. Since, the problem is confined to xz-plane only, it is found that

$$C_{12} = C_{22} = C_{23} = 0 .$$

Substituting Equations (19), (20), (21) and taking into consideration the above assumptions, Equations (17) and (18) can be rewritten in terms of the displacement components ($u_1^*, 0, u_3^*$) as

$$\left(C_{11} + P\right)\left(2\partial_{xx} u_1^* + \partial_{zz} u_1^* + \partial_{xz} u_3^*\right) + C_{13}\left(\partial_{xz} u_3^* - \partial_{zz} u_1^*\right) - 2\rho_2 g \partial_x u_3^* = 2\rho_2 \partial_{tt} u_1^*, \tag{22}$$

$$C_{11}\left(\partial_{xz} u_1^* + \partial_{xx} u_3^*\right) + \left(C_{13} + P\right)\left(\partial_{xz} u_1^* - \partial_{xx} u_3^*\right) + 2C_{33} \partial_{zz} u_3^* + 2\rho_2 g \partial_x u_1^* = 2\rho_2 \partial_{tt} u_3^*. \tag{23}$$

The displacements u_1^* and u_3^* can be derived from the displacement potentials $\phi(x, y, t)$ and $\psi(x, y, t)$ using the relations

$$u_1^* = \partial_x \phi - \partial_z \psi, \quad u_3^* = \partial_z \phi + \partial_x \psi. \tag{24}$$

Equations (22) and (23) when substituted upon by Equation (24), respectively give

$$\left(C_{11}+P\right)\nabla^2\phi-\rho_2 g\partial_x\psi=\rho_2\partial_{tt}\phi, \tag{25}$$

$$\left(C_{11}-C_{13}+P\right)\nabla^2\psi+2\rho_2 g\partial_x\phi=\rho_2\partial_{tt}\psi \tag{26}$$

and

$$C_{11}\partial_{xx}\phi+C_{33}\partial_{zz}\phi-\rho_2 g\partial_x\psi=\rho_2\partial_{tt}\phi, \tag{27}$$

$$C_{11}\left(\partial_{xx}\psi-\partial_{zz}\psi\right)-\left(C_{13}+P\right)\nabla^2\psi+2C_{33}\partial_{zz}\psi+2\rho_2 g\partial_x\phi=2\rho_2\partial_{tt}\psi, \tag{28}$$

where

$$\nabla^2=\partial_{xx}+\partial_{zz}.$$

It may be noted that, as the direction of initial compressive wave is taken along x-axis, the body wave velocities must be different in x and z directions. Thus, only Equations (25) and (28) is to be considered with a view that the wave is propagating in the direction of x only. Equations (25) and (28) correspond to compressive and shear wave respectively, along the x direction only; while Equations (26) and (27) correspond to compressive and shear wave respectively along the z direction only.

In order to solve the Equations (25) and (28), it is assumed that

$$\phi=\Phi\left(z\right)e^{ik\left(x-ct\right)}, \tag{29}$$

$$\psi=\Psi\left(z\right)e^{ik\left(x-ct\right)}. \tag{30}$$

Using Equations (29) and (30) in Equations (25) and (28) it is obtained that

$$d_{zz}\Phi+k^2M^2\Phi-i\frac{k\rho_2 g}{\alpha_1^2}\Psi=0, \tag{31}$$

$$d_{zz}\Psi+k^2N^2\Psi+i\frac{k\rho g}{\beta_1^2}\Phi=0, \tag{32}$$

where

$$M^2=\left(\frac{\rho_2c^2}{\alpha_1^2}-1\right), N^2=\left(\frac{2\rho_2c^2-C_{11}+C_{13}+P}{\beta_1^2}\right),$$
$$\alpha_1^2=C_{11}+P,\quad \beta_1^2=\left(2C_{33}-C_{11}-C_{13}-P\right). \tag{33}$$

Equation (31) and (32) suggests that

$$\left[\left(d_{zz}+k^2s_1\right)\left(d_{zz}+k^2s_2\right)\right]\left(\Phi,\Psi\right)=0, \tag{34}$$

where

$$s_1^2+s_2^2=M^2+N^2, s_1^2s_2^2=M^2N^2-\left(\frac{GC_{44}}{\beta_1\alpha_1}\right)^2. \tag{35}$$

and $G=\dfrac{\rho_2 g}{C_{44}k}$ is Biot's gravity parameter.

Now, we assume the solution of Equation (34) of the form

$$\Phi\left(z\right)=A_5^*e^{-iks_1z}+A_6^*e^{-iks_2z}+A_7^*e^{iks_1z}+A_8^*e^{iks_2z}, \tag{36}$$

where $A_5^*, A_6^*, A_7^*, A_8^*$ are arbitrary constants.

Keeping in view that the displacement vanishes as $z\to\infty$, the appropriate solution of Equations (25) and (28) may be written as

$$\phi=\left[A_5e^{-iks_1z}+A_6e^{-iks_2z}\right]e^{ik\left(x-ct\right)}, \tag{37}$$

$$\psi = \left[\bar{A}_5 e^{-iks_1 z} + \bar{A}_6 e^{-iks_2 z} \right] e^{ik(x-ct)}, \tag{38}$$

where the arbitrary constants $\bar{A}_5, \bar{A}_6$ are related to A_5, A_6 respectively by means of Equations (31) or (32).

The coefficient of $e^{-iks_1 z}$ and $e^{-iks_2 z}$ when equated to zero, Equation (31) gives

$$\bar{A}_5 = ikk_1 A_5,\ \bar{A}_6 = ikk_2 A_6,$$

where

$$k_j = \frac{\alpha_1^2 \left(s_j^2 - M^2 \right) kC_{44}}{G},\ j = 1, 2. \tag{39}$$

Therefore, the expressions for the displacement potentials are

$$\Phi = \left[A_5 e^{-iks_1 z} + A_6 e^{-iks_2 z} \right] e^{ik(x-ct)}, \tag{40}$$

$$\Psi = ik \left[A_5 k_1 e^{-iks_1 z} + A_6 k_2 e^{-iks_2 z} \right] e^{ik(x-ct)}. \tag{41}$$

So that the displacement components may be written as

$$u_1^* = \left[A_5 \left(ik - k^2 s_1 k_1 \right) e^{-iks_1 z} + A_6 \left(ik - k^2 s_2 k_2 \right) e^{-iks_2 z} \right] e^{ik(x-ct)}. \tag{42}$$

$$u_3^* = \left[A_5 \left(-iks_1 - k^2 k_1 \right) e^{-iks_1 x_3} + A_6 \left(-iks_2 - k^2 k_2 \right) e^{-iks_2 x_3} \right] e^{ik(x-ct)}. \tag{43}$$

4 BOUNDARY CONDITIONS AND SOLUTION OF THE PROBLEM

Following are the boundary conditions at the uppermost corrugated surface, and at the common corrugated as well as loosely bonded interface of layer and half-space:

(i) Traction free condition at the upper surface:

$$\tau_{33} - f_2'(x)\tau_{31} = 0,\ \tau_{13} - f_2'(x)\tau_{11} = 0, \quad \text{at} \quad z = f_2(x) - H \tag{44}$$

(ii) Condition for continuity of stresses at the common interface

$$\tau_{33} - f_1'(x)\tau_{31} = \tau_{33}^* - f_1'(x)\tau_{31}^*, \quad \tau_{13} - f_1'(x)\tau_{11} = \tau_{13}^* - f_1'(x)\tau_{11}^*, \quad \text{at } z = f_1(x) \tag{45}$$

(iii) Condition for continuity of normal displacements at the common interface

$$u_3 = u_3^*, \quad \text{at } z = f_1(x) \tag{46}$$

(iv) Condition for the proportionality of shear stress to the slip at the common interface (Vashisth et al.[1991])

$$\tau_{13} - f_1'\tau_{11} = ikC_{44} \frac{\Omega}{1-\Omega} c \sqrt{\frac{\rho_1}{\mu_T}} \left(u_1 - u_1^* \right), \text{ at } z = f_1(x) \tag{47}$$

where $\Omega (0 \le \Omega \le 1)$ is the bonding parameter. The common interface is said to be perfectly bonded for the case when $\Omega = 1$; and ideally smooth when $\Omega = 0$.

Substituting the expressions of the obtained displacement components, as given in Equations (12), (13), (42) and (43), in the above boundary conditions, six homogeneous equations in $A_j \ (j = 1, 2 \ldots, 6)$ are obtained whose non-trivial solution requires

$$\left| t_{ij} \right| = 0, \tag{48}$$

where entries t_{ij} are as provided in the Appendix. Equation (48) is the dispersion relation for the propagation of Rayleigh-type wave in a corrugated fibre-reinforced layer lying over an initially stressed orthotropic half-space under gravity.

5 NUMERICAL RESULTS AND DISCUSSION

The numerical values which have been taken into consideration with a view to perform numerical computation of phase velocity of Rayleigh-type wave propagating in a corrugated fibre-reinforced layer lying over an initially stressed orthotropic half-space under gravity, with loosely bonded common interface, are as follows:

For fibre-reinforced layer (Markham, [1970])

$$\mu_L = 7.07\times10^9 \text{ N/ m}^2,\ \mu_T = 3.5\times10^9 \text{ N/ m}^2,\ \alpha = -1.28\times10^9 \text{ N/ m}^2, \beta = 220.90\times10^9 \text{ N/ m}^2,$$
$$\lambda = 5.66\times10^9 \text{ N/ m}^2, \rho_1 = 1600\,\text{kg/m}^3.$$

For initially stressed orthotropic half-space under gravity (Prosser and Green [190])

$$C_{11} = 14.295\times10^9 \text{ N/ m}^2,\ C_{13} = 9\times10^9 \text{ N/ m}^2,\ C_{33} = 108.4\times10^9 \text{ N/ m}^2, C_{44} = 5.28\times10^9 \text{ N/ m}^2,$$
$$\rho_2 = 1442\,\text{kg/m}^3.$$

Figs. 1 to 6 irradiate the effects of undulation, corrugation, bonding of the layer and half-space, initial stress and gravity on the phase velocity of Rayleigh-type wave propagating in a fibre-reinforced layer lying over an orthotropic half-space. In all the figures, dimensionless phase velocity $\left(c\sqrt{\rho_1}\big/\sqrt{\mu_T}\right)$ has been plotted against dimensionless wave number (kH) for different values of the affecting parameters. These figures suggest that the phase velocity of Rayleigh-type wave decreases with increase in wave number.

1. Effect of Corrugated Boundary Surfaces on the Phase Velocity of Rayleigh-Type Wave

Figs. 2, 3 and 4 show the effect of corrugation and undulation on the phase velocity of Rayleigh-type wave. In particular, Fig. 2 shows the effect of corrugation parameter associated with the upper boundary surface $(a_1 b)$; Fig. 3 interprets the effect of corrugation parameter associated with the common interface of layer and half-space $(a_2 b)$; and Fig. 4 shows the effect of undulation parameter (bH) and position parameter (x/H) , on the phase velocity of Rayleigh-type wave. Curve 1 in Figs. 2 and 3 correspond to the cases when there is no corrugation in the upper boundary surface and the common interface of layer and half-space respectively. Figs. 2 and 3 elucidate that the phase velocity of Rayleigh-type wave increases with increase in the magnitude of corrugation parameter associated with the upper boundary surface whereas it decreases with increase in the magnitude of corrugation parameter associated with the common interface of layer and half-space. Comparative study of Figs. 2 and 3 suggest that the absence of corrugation in upper boundary surface disfavors the phase velocity; but the absence of corrugation at the interface of the layer and half-space greatly supports the phase velocity. The similar antagonistic behavior of corrugation on the phase velocity of Rayleigh-type wave at upper boundary surface and common interface of layer and half-space is marked by Singh et al [2016, 2017]. Fig. 4 manifests that undulation parameter along with position parameter also has great impact on the phase velocity of Rayleigh-type wave as a small increase in their magnitude significantly increases the phase velocity [Singh et al., 2017].

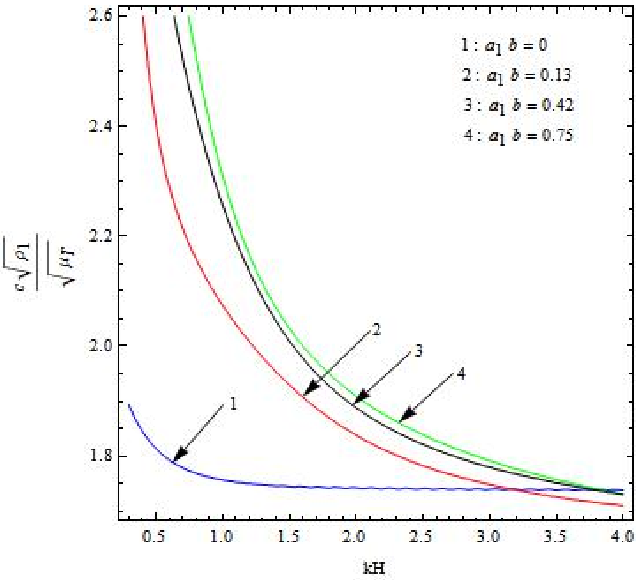

Figure 2: Variation of phase velocity $\left(c\sqrt{\rho_1}/\sqrt{\mu_T}\right)$ with wave number $\left(kH\right)$ for different values of corrugation parameter associated with the upper boundary surface $\left(a_1b\right)$.

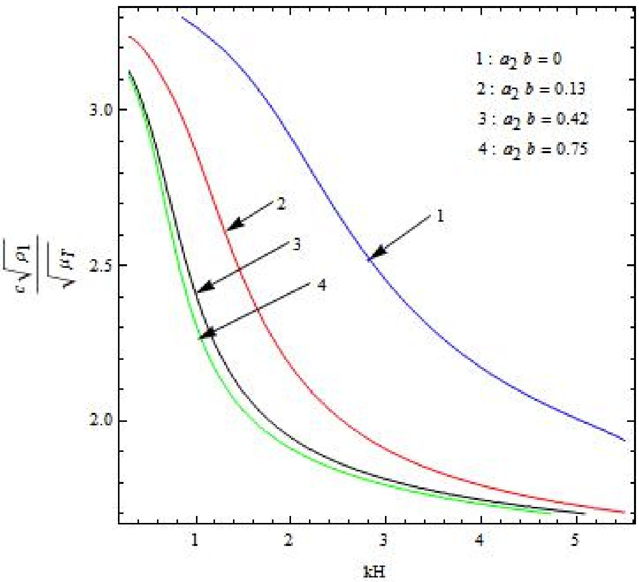

Figure 3: Variation of phase velocity $\left(c\sqrt{\rho_1}/\sqrt{\mu_T}\right)$ with wave number $\left(kH\right)$ for different values of corrugation parameter associated with the interface $\left(a_2b\right)$.

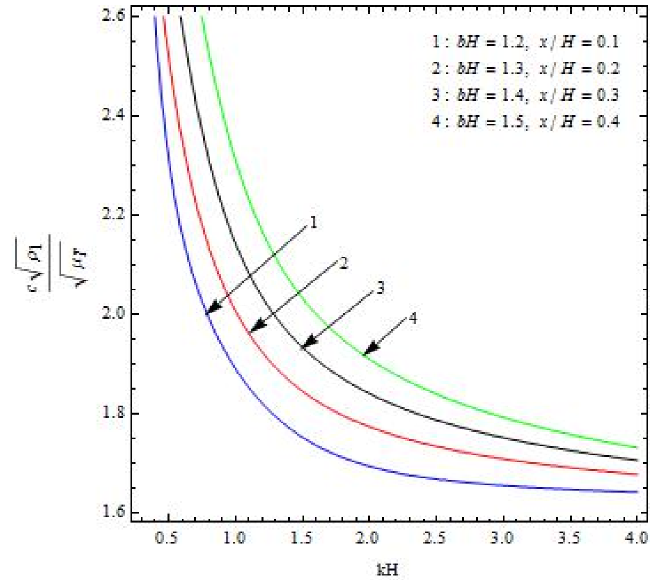

Figure 4: Variation of phase velocity $\left(c\sqrt{\rho_1}/\sqrt{\mu_T}\right)$ with wave number (kH) for different values of undulation parameter (bH) and position parameter (x/H).

2. Effect of Initial Stress on the Phase Velocity of Rayleigh-Type Wave

The effect of initial stress $(P/2C_{44})$ on the phase velocity of Rayleigh-type wave is demonstrated in Fig. 5. In this figure, curves 1 and 2 correspond to the case when the half-space is under horizontal tensile initial stress $(P/2C_{44} < 0)$; curve 3 represent the case when half-space is under no initial stress $(P/2C_{44} = 0)$; and curves 4 and 5 correspond to the case when half-space is under horizontal compressive initial stress $(P/2C_{44} > 0)$. It can be observed from the figure that the phase velocity of Rayleigh-type wave increases with increase in initial stress. Meticulous examination of the figure concludes that the phase velocity of Rayleigh-type wave decreases with increase in the magnitude of horizontal tensile initial stress; whereas it increases with increase in the magnitude of horizontal compressive initial stress. Moreover, the influence of initial stress in found significant at low frequency region as compare to the high frequency region. Similar result may be observed when the case of gravity tending to zero i.e. $(G \to 0)$ is taken in the study by Abd-Alla [1999].

3. Effect of Loose Bonding on the Phase Velocity of Rayleigh-Type Wave

The influence of loosely bonded interface of the layer and half-space on the phase velocity of Rayleigh-type wave is marked by plotting the dispersion curve for different values of bonding parameter, Ω which has been demonstrated in Fig.6. Curve 1 in the figure interprets the case when the interface of layer and half-space are near to a smooth contact $(\Omega = 0.01)$; curves 2, 3 and 4 represent that they are loosely bonded $(0 < \Omega < 1)$; and curve 5 corresponds to the case when the interface is perfectly bonded (in welded contact $(\Omega = 1)$). The figure manifests that the phase velocity decreases with increase in the magnitude of bonding parameter. Minute observation of the figure set forth the fact that, the variation of bonding parameter from loose bonding towards smooth contact mildly affects the phase velocity of Rayleigh-type wave in comparison to its variation from loose bonding towards welded contact.

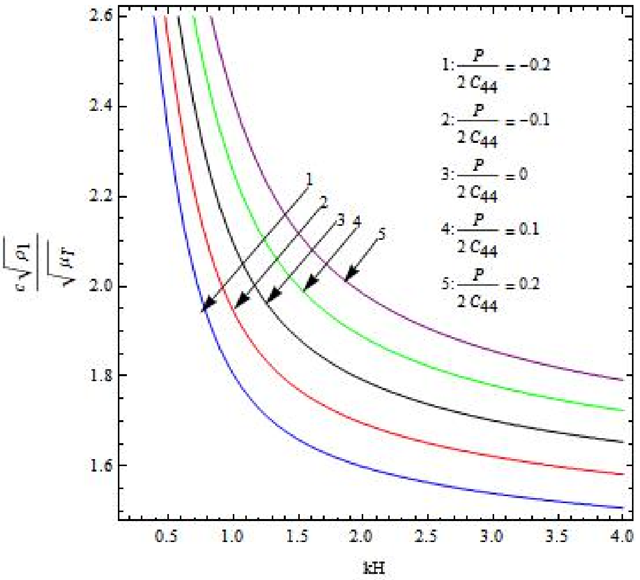

Figure 5: Variation of phase velocity $\left(c\sqrt{\rho_1}/\sqrt{\mu_T}\right)$ with wave number $\left(kH\right)$ for different values of initial stress parameter $\left(P/2C_{44}\right)$.

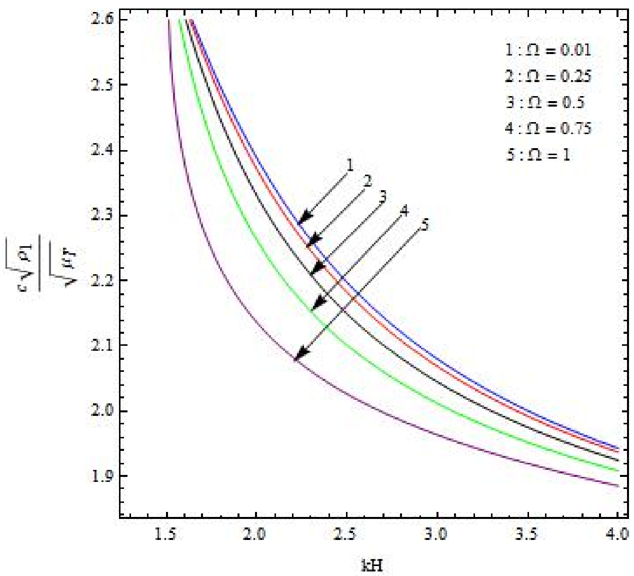

Figure 6: Variation of phase velocity $\left(c\sqrt{\rho_1}/\sqrt{\mu_T}\right)$ with wave number $\left(kH\right)$ for different values of bonding parameter $\left(\Omega\right)$.

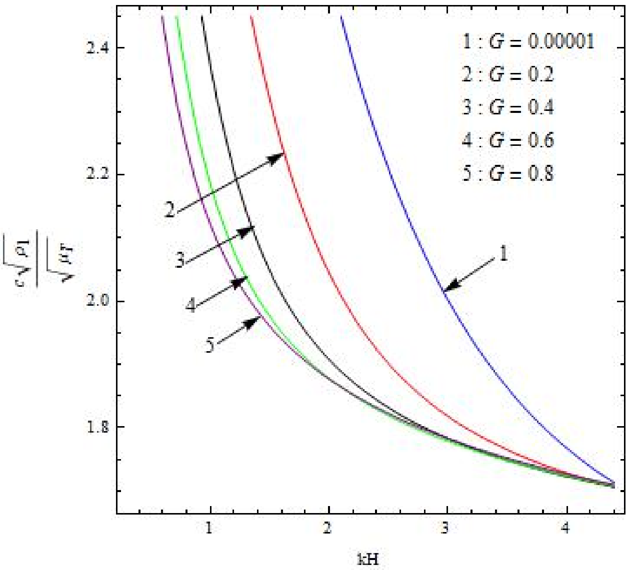

Figure 7: Variation of phase velocity $\left(c\sqrt{\rho_1}/\sqrt{\mu_T}\right)$ with wave number (kH) for different values of Biot's gravity parameter (G).

4. Effect of Gravity on the Phase Velocity of Rayleigh-Type Wave

The effect of gravity on the phase velocity of Rayleigh-type wave is shown in Fig.7. Curve 1 in this figure represents the case when effect of gravity is neglected $(G \to 0)$ whereas curve 2, 3, 4, 5 corresponds to the case when effect of gravity in increasing order is considered. It is noted from the figure that the phase velocity decreases with increase in the magnitude of Biot's gravity parameter (G) [Singh et al., 2017]. In addition to this, the figure illustrate that the impact of Biot's gravity parameter is significant at low frequency region but less at high frequency region. In fact, at high frequency region, all the curves seem to share almost a common magnitude of phase velocity.

6 CONCLUSION

The effects of undulation, corrugation, bonding of the layer and half-space, initial stress and gravity on the phase velocity of Rayleigh-type wave propagating in a corrugated fibre-reinforced layer lying over an initially stressed orthotropic half-space under gravity are investigated. The outcomes of the study are summarized as follows:

- The phase velocity of Rayleigh-type wave decreases with increase in wave number.
- The corrugation parameter associated with the upper boundary surface favors the phase velocity of Rayleigh-type wave whereas corrugation parameter associated with the common interface of layer and half-space disfavors the phase velocity of Rayleigh-type wave.
- The phase velocity Rayleigh-type wave increases with increase in undulation parameter and position parameter.
- Phase velocity of Rayleigh-type wave increases with increase in the initial stress. More precisely, phase velocity of Rayleigh-type wave decreases with increase in the horizontal tensile initial stress but it increases with increase in horizontal compressive initial stress.
- With increase in the magnitude of bonding parameter of the common interface, the phase velocity of Rayleigh-type wave decreases. In particular phase velocity of Rayleigh-type wave is maximum in case of perfect contact and least in case of smooth contact of layer and half-space
- Biot's gravity parameter disfavors the phase velocity of Rayleigh-type wave.
- Although the affecting parameters have significant effect on the phase velocity of Rayleigh-type wave yet the effect of presence and absence of corrugation at the boundary surfaces on the dispersion curve is found to be great.

The present problem may find some applications in the field of construction, civil engineering, geophysics and geomechanics. Low weight and high strength of fibre-reinforced materials makes it a crucial material for various construction works like bridges, buildings, towers, etc. The reinforcement of soil enhances the strength and load bearing capacity of it. Therefore, it is very important to study the effect of different factors on the propagation of waves through these material medium with complex geometries in view of its possible applications in diverse areas of science and engineering.

Acknowledgements

The authors convey their sincere thanks to the National Board of Higher Mathematics (NBHM) for their financial support to carry out this research work through Project NBHM/R.P. 78/2015/Fresh/ 2017/ 24.1.2017 titled "Mathematical modeling of elastic wave propagation in highly anisotropic and heterogeneous media."

References

Abd-Alla, A. M., (1999). Propagation of Rayleigh waves in an elastic half-space of orthotropic material. Applied Mathematics and Computation 99(1): 61-69.

Asano, S., (1966). Reflection and refraction of elastic waves at a corrugated interface. Bulletin of the Seismological Society of America 56 (1): 201-221.

Biot, M. A., (1965). Mechanics of Incremental Deformation, Wiley, New York.

Chai, J. F., Wu, T. T., (1996). Determination of surface wave velocities in a prestressed anisotropic solid. NDT & E Int. 29: 281–292.

Chattopadhyay, A., Gupta, S., Singh, A. K., (2009). Influence of Gravity on the Propagation of SH Waves in a Magnetoelastic Self-reinforced Media. International Journal of Mechanics and Solids 4(1): 71-83.

Chattopadhyay, A., Gupta, S., Singh, A. K., (2010). The dispersion of shear wave in multi-layered magnetoelastic self-reinforced media. International Journal of Solids and Structure 47(9): 1317-1324.

Chattopadhyay, A., Singh, A. K., (2012) Propagation of magnetoelastic shear waves in an irregular self-reinforced layer. Journal of Engineering Mathematics 75: 139-155.

Chattopadhyay, A., Singh, A. K., (2013). Propagation of a crack due to magnetoelastic shear waves in a self-reinforced medium. Journal of Vibration and Control 20(3): 406-420.

Chow, T. S., (1971). On the propagation of flexural waves in an orthotropic laminated plate and its response to an impulsive load. Journal of Composite Materials 5(3): 306-319.

Das, S. C., Acharya, D. P., Sengupta, D. R., (1992). Surface waves in an inhomogeneous elastic medium under the influence of gravity. Rev Roumaine Sci Tech Ser Mec Appl 37: 539–551.

Destrade, M., (2001). Surface waves in orthotropic incompressible materials. Journal of the Acoustical Society of America 110(2): 837-840.

Fan, C. W., Hwu, C. (1998). Rigid stamp indentation on a curvilinear hole boundary of an anisotropic elastic body. Journal of applied mechanics 65(2): 389-397.

Grünewald, S., Laranjeira, F., Walraven, J., Aguado, A., Molins, C., (2012). Improved tensile performance with fiber reinforced self-compacting concrete. High Performance Fiber Reinforced Cement Composites 6: 51-58.

Gaur, A. M., Rana, D. S., (2014). Shear wave propagation in piezoelectric-piezoelectric composite layered structure. Latin American Journal of Solids and Structures 11(13): 2483-2496.

Khurana, P., Vashisth, A. K., (2001). Love wave propagation in a pre-stressed medium. Indian Journal of Pure and Applied Mathematics 32(8): 1201-1208.

Kumar, R., Kumar, R., (2011). Analysis of wave motion at the boundary surface of orthotropic thermoelastic material with voids and isotropic elastic half-space. Journal of Engineering Physics and Thermophysics 84(2): 463-478.

Markham, M. F., (1970). Measurements of Elastic constants of fibre composites. Ultrasonics 1: 145-149.

Munish, S., Sharma, A., Sharma, A., (2016). Propagation of SH Waves in a Double Non-Homogeneous Crustal Layers of Finite Depth Lying Over an homogeneous Half-Space. Latin American Journal of Solids & Structures 13(14): 2628-2642.

Nandal, J. S., Saini, T. N., (2013). Reflection and refraction at an imperfectly bonded interface between poroelastic solid and cracked elastic solid. Journal of Seismology 17(2): 239-253.

Prikazchikov, D. A., Rogerson, G. A., (2003). Some comments on the dynamic properties of anisotropic and strongly anisotropic prestressed elastic solids. International Journal of Engineering Science 41: 149–171.

Prosser, W. H., Green, R. E., (1990). Characterization of the nonlinear elastic properties of graphite/epoxy composites using ultrasound. Journal of Reinforced Plastics and Composites 9(2): 162-173.

Samal, S., Chattaraj, R., (2011). Surface wave propagation in fiber-reinforced anisotropic elastic layer between liquid saturated porous half space and uniform liquid layer. Acta Geophysica 59(3): 470-482.

Singh, B., Kumar, R., (1998). Reflection and refraction of micropolar elastic waves at a loosely bonded interface between viscoelastic solid and micropolar elastic solid. International Journal of Engineering Science 36(2): 101-117.

Singh, S. S., Tomar, S. K., (2008). qP-wave at a corrugated interface between two dissimilar pre-stressed elastic half-spaces. Journal of Sound and Vibration 317(3): 687-708.

Singh, S. S., (2011). Love wave at a layer medium bounded by irregular boundary surfaces. Journal of Vibration and Control 17(5): 789-795.

Singh, B., Yadav, A. K., (2013). Reflection of plane waves in an initially stressed perfectly conducting transversely isotropic solid half-space. Journal of Earth System and Science 122(4): 1045-1053.

Singh, S. S., (2014). Reflection and Transmission of Elastic Waves at a Loosely Bonded Interface between an Elastic Solid and a Viscoelastic Porous Solid Saturated by Viscous Liquid. Global Journal of Researches in Engineering 14(3).

Singh, A. K., Das, A., Kumar, S., Chattopadhyay, A., (2015). Influence of corrugated boundary surfaces, reinforcement, hydrostatic stress, heterogeneity and anisotropy on Love-type wave propagation. Meccanica 50(12): 2977-2994.

Singh, A. K., Mistri, K. C., Das, A., (2016). Propagation of Love-type wave in a corrugated fibre-reinforced layer. Journal of Mechanics 32(6): 693-708.

Singh, A. K., Mistri, K. C., Kaur, T., Chattopadhyay, A., (2017). Effect of undulation on SH-wave propagation in corrugated magneto-elastic transversely isotropic layer. Mechanics of Advanced Materials and Structures 24(3): 200-211.

Spencer, A. J. M., (1972). Deformations of fibre-reinforced materials. Oxford University Press, New York.

Tomar, S. K., Kaur, J., (2007). SH-waves at a corrugated interface between a dry sandy half-space and an anisotropic elastic half-space. Acta Mechanica 190(1-4): 1-28.

Vashisth, A. K., Sharma, M. D., Gogna, M. L., (1991) Reflection and transmission of elastic waves at a loosely bonded interface between an elastic solid and liquid-saturated porous solid. Geophysical journal international 105(3): 601-617.

APPENDIX

$$t_{11} = \left[-\varsigma_1\gamma_1(\lambda+2\mu_T)+\mu_T f_2'\gamma_1+i(\lambda+\alpha-f_2'\varsigma_1\mu_T)\right]e^{-k\gamma_1(f_2-H)},$$

$$t_{12} = \left[-\varsigma_2\gamma_2(\lambda+2\mu_T)+\mu_T f_2'\gamma_2+i(\lambda+\alpha-f_2'\varsigma_2\mu_T)\right]e^{-k\gamma_2(f_2-H)},$$

$$t_{13} = \left[-\varsigma_1\gamma_1(\lambda+2\mu_T)-\mu_T f_2'\gamma_1+i(\lambda+\alpha+f_2'\mu_T\varsigma_1)\right]e^{k\gamma_1(f_2-H)},$$

$$t_{14} = \left[-\varsigma_2\gamma_2(\lambda+2\mu_T)-\mu_T f_2'\gamma_2+i(\lambda+\alpha+f_2'\varsigma_2\mu_T)\right]e^{k\gamma_2(f_2-H)},\quad t_{15}=0,\ t_{16}=0,$$

$$t_{21} = \left[-\mu_T\gamma_1+f_2'\varsigma_1\gamma_1(\lambda+\alpha)+i\left\{\mu_T\varsigma_1-(\lambda+2\alpha+4\mu_L-2\mu_T+\beta)f_2'\right\}\right]e^{-k\gamma_1(f_2-H)},$$

$$t_{22} = \left[-\mu_T\gamma_2+f_2'\varsigma_2\gamma_2(\lambda+\alpha)+i\left\{\mu_T\varsigma_2-(\lambda+2\alpha+4\mu_L-2\mu_T+\beta)f_2'\right\}\right]e^{-k\gamma_2(f_2-H)},$$

$$t_{23} = \left[\mu_T\gamma_1+f_2'\varsigma_1\gamma_1(\lambda+\alpha)+i\left\{-\mu_T\varsigma_1-(\lambda+2\alpha+4\mu_L-2\mu_T+\beta)f_2'\right\}\right]e^{k\gamma_1(f_2-H)},$$

$$t_{24} = \left[\mu_T\gamma_2+f_2'\varsigma_2\gamma_2(\lambda+\alpha)+i\left\{-\mu_T\varsigma_2-(\lambda+2\alpha+4\mu_L-2\mu_T+\beta)f_2'\right\}\right]e^{k\gamma_2(f_2-H)},$$

$$t_{25}=0,\quad t_{26}=0,\quad t_{31} = \left[-\varsigma_1\gamma_1(\lambda+2\mu_T)+\mu_T f_1'\gamma_1+i(\lambda+\alpha+\varsigma_1 f_1'\mu_T)\right]e^{-k\gamma_1 f_1},$$

$$t_{32} = \left[-\varsigma_2\gamma_2(\lambda+2\mu_T)+\mu_T f_1'\gamma_2+i(\lambda+\alpha-\varsigma_2 f_1'\mu_T)\right]e^{-k\gamma_2 f_1},$$

$$t_{33} = \left[-\varsigma_1\gamma_1(\lambda+2\mu_T)-\mu_T f_1'\gamma_1+i\left\{\lambda+\alpha+\mu_T f_1'\varsigma_1\right\}\right]e^{k\gamma_1 f_1},$$

$$t_{34} = \left[-\varsigma_2\gamma_2(\lambda+2\mu_T)-\mu_T f_1'\gamma_2+i(\lambda+\alpha+\varsigma_2 f_1'\mu_T)\right]e^{k\gamma_2 f_1},$$

$$t_{35} = -\left[k\left(-C_{13}+C_{33}s_1^2-2f_1'C_{44}s_1\right)+ik^2k_1\left(-C_{13}s_1+C_{33}s_1-f_1'C_{44}s_1^2+f_1'C_{44}\right)\right]e^{-iks_1 f_1},$$

$$t_{36} = -\left[k\left(-C_{13}+C_{33}s_2^2-2f_1'C_{44}s_2\right)+ik^2k_2\left(-C_{13}s_2+C_{33}s_2-f_1'C_{44}s_2^2+f_1'C_{44}\right)\right]e^{-iks_2 f_1},$$

$$t_{41} = \left[-\mu_T\gamma_1+f_1'\varsigma_1\gamma_1(\lambda+\alpha)+i\left\{\mu_T\varsigma_1-(\lambda+2\alpha+4\mu_L-2\mu_T+\beta)f_1'\right\}\right]e^{-k\gamma_1 f_1},$$

$$t_{42} = \left[-\mu_T\gamma_2+f_1'\varsigma_2\gamma_2(\lambda+\alpha)+i\left\{\mu_T\varsigma_2-(\lambda+2\alpha+4\mu_L-2\mu_T+\beta)f_1'\right\}\right]e^{-k\gamma_2 f_1},$$

$$t_{43} = \left[\mu_T\gamma_1+f_1'\varsigma_1\gamma_1(\lambda+\alpha)+i\left\{-\mu_T\varsigma_1-(\lambda+2\alpha+4\mu_L-2\mu_T+\beta)f_1'\right\}\right]e^{k\gamma_1 f_1},$$

$$t_{44} = \left[\mu_T\gamma_2+f_1'\varsigma_2\gamma_2(\lambda+\alpha)+i\left\{-\mu_T\varsigma_2-(\lambda+2\alpha+4\mu_L-2\mu_T+\beta)f_1'\right\}\right]e^{k\gamma_2 f_1},$$

$$t_{45} = -\left[2C_{44}ks_1+f_1'(C_{11}+P)k+f_1'(C_{13}+P)ks_1^2+ik^2k_1\left\{C_{44}s_1^2-C_{44}+f_1'(C_{11}+P)s_1-f_1'(C_{13}+P)s_1\right\}\right]e^{-iks_1 f_1},$$

$$t_{46} = -\Big[2C_{44}ks_2+f_1'(C_{11}+P)k+f_1'(C_{13}+P)ks_2^2$$
$$+ik^2k_2\left\{C_{44}s_2^2-C_{44}+f_1'(C_{11}+P)s_2-f_1'(C_{13}+P)s_2\right\}\Big]e^{-iks_2 f_1},$$

$$t_{51}=\varsigma_1 e^{-k\gamma_1 f_1},\ t_{52}=\varsigma_2 e^{-k\gamma_2 f_1},\ t_{53}=-\varsigma_1 e^{k\gamma_1 f_1},\ t_{54}=-\varsigma_2 e^{k\gamma_2 f_1},\ t_{55}=\left(k^2k_1+s_1ki\right)e^{-iks_1 f_1},\ t_{56}=\left(k^2k_2+s_2ki\right)e^{-iks_2 f_1},$$

$$t_{61} = \left[-\mu_T\gamma_1 k-ikC_{44}\frac{\Omega}{1-\Omega}c\sqrt{\frac{\rho_1}{\mu_T}}+f_1'\varsigma_1\gamma_1 k(\lambda+\alpha)+ik\left\{\mu_T\varsigma_1-(\lambda+2\alpha+4\mu_L-2\mu_T+\beta)f_1'\right\}\right]e^{-k\gamma_1 f_1},$$

$$t_{62} = \left[-\mu_T\gamma_2 k-ikC_{44}\frac{\Omega}{1-\Omega}c\sqrt{\frac{\rho_1}{\mu_T}}+f_1'\varsigma_2\gamma_2 k(\lambda+\alpha)+ik\left\{\mu_T\varsigma_2-(\lambda+2\alpha+4\mu_L-2\mu_T+\beta)f_1'\right\}\right]e^{-k\gamma_2 f_1},$$

$$t_{63} = \left[\mu_T\gamma_1 k-ikC_{44}\frac{\Omega}{1-\Omega}c\sqrt{\frac{\rho_1}{\mu_T}}+f_1'\varsigma_1\gamma_1 k(\lambda+\alpha)+ik\left\{-\mu_T\varsigma_1-(\lambda+2\alpha+4\mu_L-2\mu_T+\beta)f_1'\right\}\right]e^{k\gamma_1 f_1},$$

$$t_{64}=\left[\mu_T k\gamma_2 - ikC_{44}\frac{\Omega}{1-\Omega}c\sqrt{\frac{\rho_1}{\mu_T}}+f_1'\varsigma_2\gamma_2 k\left(\lambda+\alpha\right)+ik\left\{-\mu_T\varsigma_2-\left(\lambda+2\alpha+4\mu_L-2\mu_T+\beta\right)f_1'\right\}\right]e^{k\gamma_2 f_1},$$

$$t_{65}=ikC_{44}\frac{\Omega}{1-\Omega}\left(-ks_1k_1+i\right)e^{-iks_1 f_1},\quad t_{66}=ikC_{44}\frac{\Omega}{1-\Omega}\left(-ks_2k_2+i\right)e^{-iks_2 f_1}.$$